A Point-to-multipoint Flexible Transceiver for Inherently Hub-and-Spoke IMDD Optical Access Networks

Chen, Lin; Jin, Wei; He, Jiaxiang; Giddings, Roger; Huang, Yi; Tang, Jianming

Journal of Lightwave Technology

DOI:
10.1109/JLT.2023.3249406

Published: 15/07/2023

Peer reviewed version

A Point-to-multipoint Flexible Transceiver for Inherently Hub-and-Spoke IMDD Optical Access Networks

Lin Chen, Wei Jin, Jiaxiang He, Roger Philip Giddings, *Member, IEEE*, Yi Huang, and Jianming Tang *Member, IEEE*

***Abstract*— Point-to-multipoint (P2MP) transceivers offer a promising solution to transform present point-to-point optical access networks into scalable and flexible P2MP networks capable of dynamically meeting, in a cost-effective and high energy consumption efficiency manner, the requirements associated with 5G-Advance and beyond networks, including large signal transmission capacity, fast and dense connection, high network flexibility/adaptability and low latency. However, the previously reported P2MP optical transceivers based on either coherent XR optics or IMDD digital filter multiplexing (DFM) techniques are not suitable for implementing in low-latency and highly cost-sensitive IMDD-dominated optical access networks. This paper proposes, experimentally demonstrates and optimises a novel P2MP flexible transceiver incorporating a new cascaded IFFT/FFT-based multi-channel aggregation/de-aggregation technique and an orthogonal digital filtering technique. The performances of the proposed technique are extensively evaluated experimentally in an upstream 55.3Gb/s @25km IMDD PON. It is shown that in comparison with the conventional DFM transceivers, the proposed transceivers can reduce the transmitter DSP complexity by a factor that approximates to aggregated channel count, and simultaneously offer additional physical layer network security, without requiring long digital filter lengths and greatly compromising upstream transmission performances/spectral efficiencies as well as differential ONU launch power dynamic ranges.**

***Index Terms*— point-to-multipoint (P2MP) transceivers, multi-channel aggregation, digital orthogonal filtering, intensity modulation and direct detection (IMDD).**

This work was part-funded by the European Regional Development Fund through Welsh Government, part-funded by the North Wales Growth Deal through Ambition North Wales, Welsh Government and UK Government, part-funded by the China Scholarship Council (202008310010), part-funded by the Science and Technology Commission of Shanghai Municipality Project Grant (SKLSFO2021-02), part-funded by the National Key Research and Development Program of China (2022YFF0708400), and part-funded by the Natural Science Foundation of Shanghai (22ZR1423000). (*Corresponding author: Wei Jin*)

Lin Chen is with College of Electronics and Information Engineering, Shanghai University of Electric Power, 200090, Shanghai, China. (email: chenlin1008@shiep.edu.cn).

Lin Chen, Wei Jin, Jiaxiang He, Roger Philip Giddings, and Jianming Tang are with the School of Electronic Engineering, Bangor University, Bangor, LL57 1UT, UK. (email: w.jin@bangor.ac.uk ; j.tang@bangor.ac.uk).

Yi Huang is with Key Laboratory of Specialty Fiber Optics and Optical Access Networks, Shanghai University, 200444, Shanghai, China. (email: huangyi1008@shu.edu.cn)

I. Introduction

The advent of 5G-Advance and beyond networks fuels the exponential data traffic growth and drives the need for innovation to significantly reduce optical access network's capital expenditure (CapEx) and operation expense (OpEx) [1, 2]. In the 5G-Advance and beyond era, a large number of emerging traffic-intensive and highly interactive applications with significantly differentiated connectivity, bandwidth, and latency requirements, such as augmented reality and Internet of Things, impose additional stringent requirements on future optical access networks with regard to network elasticity, flexibility and adaptability [3, 4].

Present optical access networks including passive optical networks (PONs) and 5G X-hauls are inherently hub-and-spoke, where a large number of spoke nodes at different locations are connected to a single hub node [5, 6]. However, representative conventional optical technologies just offer point-to-point (P2P) connections between the spoke and hub nodes and each established spoke-hub connection utilizes two dedicated P2P transceivers operating at the same predefined speeds [7]. Due to its inefficient network resource utilization, the existing P2P technologies are expensive for satisfying the above stringent requirements of 5G-Advance and beyond networks [8].

To effectively solve the challenges, point-to-multipoint (P2MP) transceivers have attracted huge R&D attention [8-10]. The P2MP transceivers allow a large number of low-speed spoke transceivers at different locations to concurrently communicate with far fewer high-speed hub transceivers concentrated at a single hub node [9, 10]. In comparison with the conventional P2P transceivers, such P2MP transceivers can not only reduce hub transceiver count by 50% but also eliminate intermediate packet aggregation stages and decrease power consumption and footprint [11]. Thus the transceiver can give rise to >70% reductions in CapEx and OpEx [11]. Furthermore, it can also dynamically provide fast P2MP logical connectivity over arbitrary physical network pathologies, and each connection can be adaptively tailored to an individual service/application with a specific bandwidth demand and traffic pattern [11]. By making use of the P2MP transceivers, present P2P optical access networks can be transformed into scalable and flexible P2MP networks, which offer a promising solution capable of meeting the capacity, connectivity, and

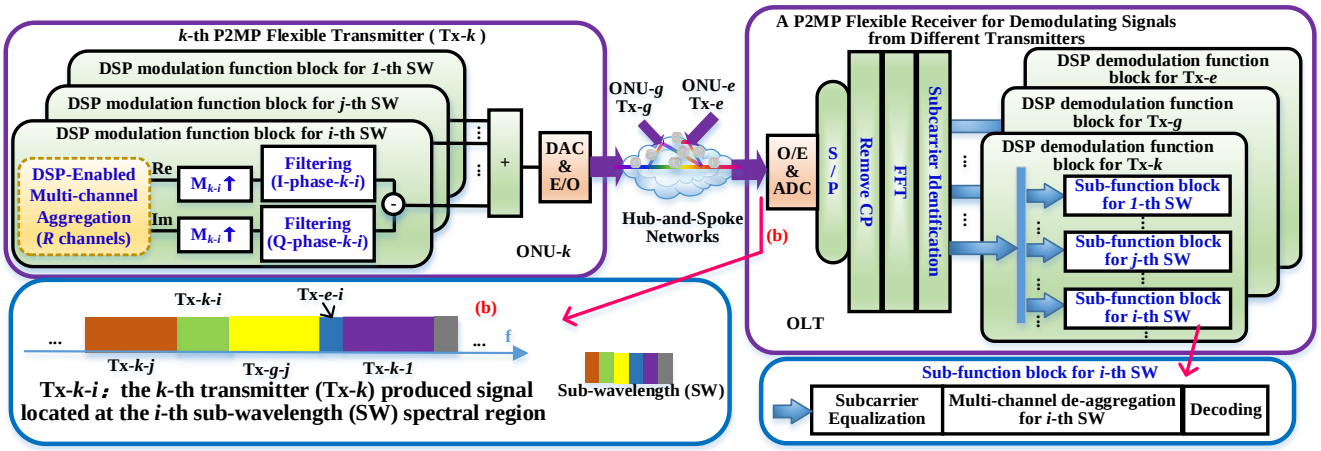

Fig. 1 Schematic diagram of an illustrative hub-and-spoke IMDD optical access network incorporating the proposed P2MP flexible transceivers.

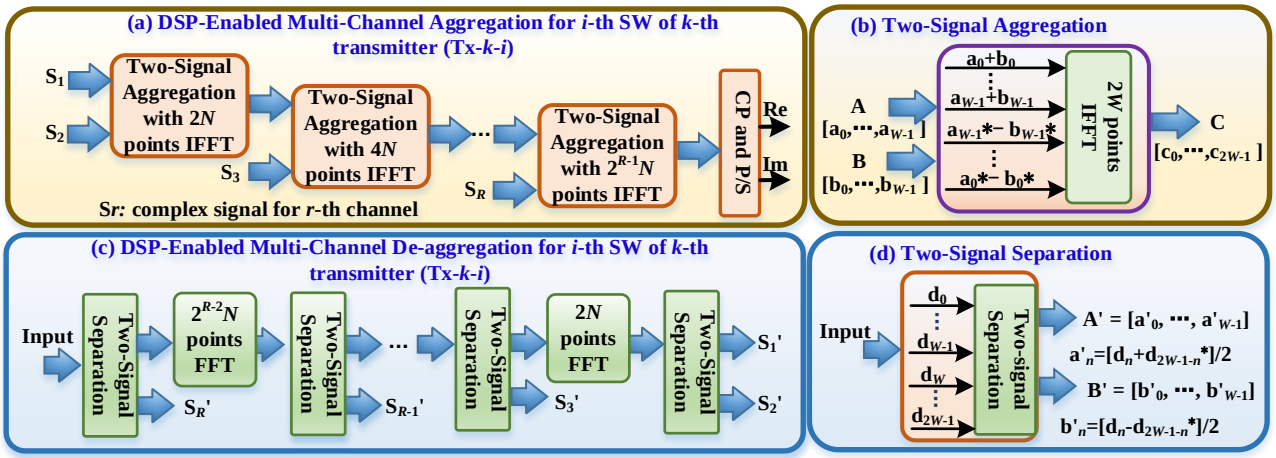

Fig. 2 Operating principle of the new IFFT/FFT-based multi-channel aggregation/de-aggregation technique embedded in the proposed P2MP flexible transceivers. (a) and (b) multi-channel aggregation, (c) and (d) multi-channel de-aggregation.

flexibility requirements of 5G-Advance and beyond networks [12].

Recently, two categories of P2MP transceivers respectively based on coherent technology [11-14] and intensity modulation and direct detection (IMDD) technology [15-20] have been reported. XR optics incorporating coherent technologies and digital subcarrier multiplexing offers a representative coherent solution for delivering the highly desirable P2MP transceivers [11]. The digital subcarrier multiplexing techniques are used for realizing multi-channel aggregations [12], and the coherent technologies are utilized for achieving both optical modulation and optical filter-free selection/detection of targeted channels [13]. However, the installed optical access networks are dominated by IMDD technologies, this hinders the practical deployment of the coherent XR optics technologies in the present optical access networks. On the other hand, digital filter multiplexing (DFM) transceivers provide a cost-effective IMDD solution for achieving P2MP transceivers without requiring huge modifications in existing network infrastructures [15, 16]. For the DFM techniques, orthogonal digital filtering is used for achieving gapless multi-channel aggregations with negligible channel interference effects. While for realizing multi-channel de-aggregations, use can be made of either fast Fourier transform (FFT) operations [17-20] or orthogonal digital filtering operations [15, 16]. However, for the DFM technique, the increase of accommodated channels can lead to an exponential growth in transmitter digital signal processing (DSP) complexity. The large transmitter DSP complexity unavoidably results in a relatively long time delay and high CapEx and OpEx.

To effectively solve the above technique issues, in this paper, a novel P2MP flexible transceiver is proposed, experimentally demonstrated and extensively evaluated in an upstream 55.3Gbps@25km IMDD PON. This transceiver incorporates a new cascaded inverse fast Fourier transform (IFFT)/FFT-based multi-channel aggregation/de-aggregation technique and an orthogonal digital filtering technique. The IFFT/FFT-based multi-channel aggregation/de-aggregation technique can considerably reduce the transceiver DSP complexity, whilst the orthogonal digital filtering technique is used to locate signals at desirable radio frequency spectral regions and simultaneously improve network spectral efficiency.

Similar to the coherent XR optics and IMDD DFM techniques, the proposed technique has the potential of transforming the present optical access networks into frequency division multiplexing (FDM) networks. It can thus maintain the

salient features associated with the above two techniques including excellent network upgradability and scalability, and effective mitigation of high latency and latency jitter issues associated with time division multiplexing (TDM) networks [12, 21].

In comparison with the coherent XR optics, the proposed transceivers are suitable for IMDD-based optical access networks and have additional advantages including: 1) allowing the use of installed free-running lasers without requiring narrow laser linewidth and precisely locking laser central frequency, 2) allowing transceivers to operate at an arbitrary speed, especially at very low speeds, and 3) simplified DSP-based signal equalizations.

In comparison with the DFM transceivers, the proposed transceivers can not only reduce the transmitter DSP complexity by a factor that approximates to aggregated channel count but also offer additional physical layer network security. Furthermore, the measured upstream PON experimental results also show that the DFM technique and the new technique present similar requirements on orthogonal digital filter characteristics and can deliver similar upstream transmission performances, and upstream transmission spectral efficiency as well as differential optical network unit (ONU) optical launch power dynamic ranges. All the above advantages of the proposed techniques are achievable without requiring extra optical and electrical components.

II. Theoretical Model and Operating Principle of P2MP Flexible Transceivers

An illustrative hub-and-spoke optical access network incorporating the proposed P2MP flexible transceivers is illustrated in Fig. 1, in which multiple P2MP flexible transmitters in ONUs can concurrently communicate to a single P2MP flexible receiver in an optical line terminal (OLT). Each P2MP transmitter uses multiple radio frequency spectral regions, termed sub-wavelengths in this paper, to transmit different signals, and each signal occupying an individual sub-wavelength may contain an arbitrary number of independent channels. As shown in the signal spectrum of Fig. 1, different sub-wavelengths can have different spectral bandwidths without any guard bands between adjacent sub-wavelengths.

A. Transmitter Operating Principle

The P2MP flexible transmitter design illustrated in Fig. 1 contains multiple DSP modulation function blocks in parallel. Each DSP modulation function block can produce an individual real-valued signal containing an arbitrary number of independent channels located at a specific sub-wavelength desired. In each DSP modulation function block, a multi-channel aggregation operation, a digital up-sampling operation and digital filtering operations are successively performed.

To detail the operating principle of the proposed P2MP flexible transmitters, the *k*-th P2MP flexible transmitter-embedded DSP modulation function block for the *i*-th sub-wavelength is explicitly explained below. Firstly, the DSP-enabled multi-channel aggregation operation is performed to produce a complex-valued baseband signal containing *R* independent channels using the DSP-enabled multi-channel aggregation technique outlined in Fig. 2(a) and Fig. 2(b). For this multi-channel aggregation technique, the aggregation of *R* independent channels requires to perform (*R*-1) cascaded IFFT operations. To aggregate the *r*-th channel, the IFFT size of the (*r*-1)-th IFFT operation is given by,

$$L_{IFFT\_(r-1)} = 2W = 2^{r-1}N, \quad r = [2,..,R] \tag{1}$$

where 2*N* is the size of the first IFFT operation. *W* is the size of the two signals to be aggregated by the (*r*-1)-th IFFT operation. It can be found that the *r*-th IFFT operation size doubles the size of the (*r*-1)-th IFFT operation.

As seen in Fig. 2(b), assuming the two signals to be aggregated by the (*r*-1)-th IFFT operation are $A=[a_0, a_1,\ldots, a_{W-1}]$ and $B=[b_0, b_1,\ldots, b_{W-1}]$ and the signal *A* is the output of the (*r*-2)-th IFFT operation, the input to the (*r*-1)-th IFFT operation can thus be expressed as,

$$S_{IFFT\_(r-1)}(n) = \begin{cases} a_n + b_n, & n = 0,1,...,W-1 \\ a^*_{2W-1-n} - b^*_{2W-1-n}, & n = W, W+1,...,2W-1 \end{cases} \tag{2}$$

where * stands for the conjugate operation. a_n is the *n*-th sample of the output of the (*r*-2)-th IFFT operation. b_n is the *n*-th sample of the *r*-th channel-transmitted signal coded by any signal modulation formats such as m-ary quadrature amplitude modulation or phase-shift keying (m-QAM or m-PSK). After having aggregated the *R* independent channels, a cyclic prefix (CP) insertion operation and a parallel-to-serial conversion (P/S) operation are performed successively.

Subsequently, to locate the resulting signal at a targeted *i*-th sub-wavelength, the resulting complex-valued baseband signal, $x_{k\_i}(t)$, undergoes a digital up-sampling operation and an orthogonal digital filtering operation, which can be described as,

$$\begin{aligned} y_{k\_i}(t) = {} & M_{k\_i}\uparrow\{\mathrm{Re}(x_{k\_i}(t))\} \otimes h^I_{k\_i}(t) - \\ & M_{k\_i}\uparrow\{\mathrm{Im}(x_{k\_i}(t))\} \otimes h^Q_{k\_i}(t) \end{aligned} \tag{3}$$

where $\mathrm{Re}(x_{k\_i}(t))$ and $\mathrm{Im}(x_{k\_i}(t))$ denote the real part and the imaginary part of the complex-valued input signal, $x_{k\_i}(t)$, respectively. $M_{k\_i}\uparrow$ represents the digital up-sampling operation with an up-sampling factor of M_{k_i} [22]. $\{ h^I_{k\_i}(t),\ h^Q_{k\_i}(t) \}$ stand for the *k*-th P2MP flexible transmitter-embedded orthogonal digital filter pairs used to locate the corresponding signal at the *i*-th sub-wavelength. The superscripts of *I* and *Q* indicate the in-phase and quadrature-phase digital filter types [22]. $y_{k\_i}(t)$ is the produced real-valued radio frequency signal located at the *i*-th sub-wavelength and contains *R* independent channels.

Finally, after combining all digitally filtered signals produced by different DSP modulation function blocks, an electrical-optical (E-O) conversion can thus be performed to generate an optical signal.

B. Receiver Operating Principle

The P2MP flexible receivers are illustrated in Fig. 1, which are capable of simultaneously demodulating different signals from various P2MP flexible transmitters. It can be found that the P2MP receiver DSP contains multiple DSP demodulation function blocks each used to demodulate the signals from a specific P2MP flexible transmitter. Because a P2MP flexible transmitter can transmit multiple signals over different sub-wavelengths, thus each DSP demodulation function block consists of multiple sub-function blocks each used to demodulate a signal at a specific sub-wavelength.

As seen in Fig. 1, in the receiver DSP, after serial-to-parallel (S/P) conversion and CP removal, the FFT operations are performed to separate all received signals at the different sub-wavelengths. To recover the received signal produced by the DSP modulation function block of the *i*-th sub-wavelength in the *k*-th flexible transmitter, its required FFT operation size satisfies,

$$L_{FFT\_k\_i} = M_{k\_i} \bullet P, \text{ where } P = 2^{R-1} N \tag{4}$$

where P is the size of the last IFFT operation utilized in the corresponding multi-channel aggregation operation. If all the received signals at different sub-wavelengths require the same FFT size, a single FFT operation is sufficient to separate all the received signals from these transmitters. When different signals at different sub-wavelengths require different FFT sizes, multiple FFT operations need to be implemented and each FFT operation corresponds to a specific FFT size. Such FFT operations for separating the received signals at different sub-wavelengths are similar to the receiver DSP procedure reported in [20]. After signal separation, a subcarrier identification process is then performed to identify the subcarriers at individual sub-wavelengths following the DSP procedures reported in [20]. According to the sub-wavelength allocations in each P2MP flexible transmitter, the subcarriers from different P2MP flexible transmitters can be identified in the receiver. All the subcarriers identified from a specific P2MP flexible transmitter are then passed to their corresponding DSP demodulation function block. In each DSP demodulation function block, the subcarriers of each individual sub-wavelength successively undergo a subcarrier equalization operation, a multi-channel de-aggregation operation and a decoding operation.

In the subcarrier equalization process, the conventional single-tap equalizer [17] can be employed to compensate for the subcarrier signal distortions. Subsequently, the multi-channel de-aggregation operation illustrated in Fig. 2(c) and Fig. 2(d) is performed for separating the aggregated channels for each individual sub-wavelength. To recover the data conveyed by the *i*-th sub-wavelength of the *k*-th P2MP flexible transmitter, assuming that the transmitted signal contains R independent channels, in the receiver DSP, as seen in Fig. 2(c), separating the aggregated R channels needs to perform (R-2) FFT operations and (R-1) two-signal separation operations. For example, to separate the r-th channel, as depicted in Fig. 2(d), the input to the corresponding two-signal separation operation is $D=[d_0,.., d_{W-1}, d_W,.., d_{2W-1}]$, which can be expressed as,

$$d(n) = \begin{cases} a'_n + b'_n, & n = 0,..,W-1 \\ a'^{*}_{2N-1-n} - b'^{*}_{2N-1-n}, & n = W,..,2W-1 \end{cases} \tag{5}$$

At the output of the two-signal separation operation, the two signals, $A'=[a'_0,.., a'_{W-1}]$ and $B'=[b'_0,.., b'_{W-1}]$, can thus be obtained by,

$$\begin{cases} a'_n = \frac{1}{2}\left[d_n + d^{*}_{2N-1-n} \right] \\ b'_n = \frac{1}{2}\left[d_n - d^{*}_{2N-1-n} \right] \end{cases}, \text{ where } n = 0,..,W-1 \tag{6}$$

where the signal B' is the received signal transmitted over the r-th channel. The signal A' is the input to the following FFT operation for the (r-1)-th channel de-aggregation.

The above-described P2MP flexible transceivers would potentially operate in an ‘add-as-you-grow’ mode. Controlled by software-defined networking (SDN), the optical network-accommodated transmitter count and each transmitter-allocated sub-wavelength count, as well as each sub-wavelength-accommodated channel count, can be made variable adaptively according to the actual user requirements. Adding new transmitters or activating/inactivating specific transmitters only requires creating new or activating/inactivating the corresponding DSP demodulation function blocks in the hub receiver DSP without needing to modify all other existing transmitters. Furthermore, for each individual transmitter, dynamic variations in both the sub-wavelength count and each sub-wavelength channel count can also be made adaptive according to actual user requirements. As seen in Fig. 1, for a specific transmitter, dynamic sub-wavelength count variations are achievable by simultaneously activating/inactivating the transmitter DSP modulation function blocks of the specific sub-wavelengths and the corresponding receiver DSP sub-function blocks. Moreover, for each sub-wavelength of a specific transmitter, dynamic channel count variations are also realizable by dynamically increasing/decreasing the corresponding two-signal aggregation module count in the transmitter multi-channel aggregation operation and simultaneously altering the FFT module count and the two-signal separation module count in the receiver multi-channel de-aggregation operation.

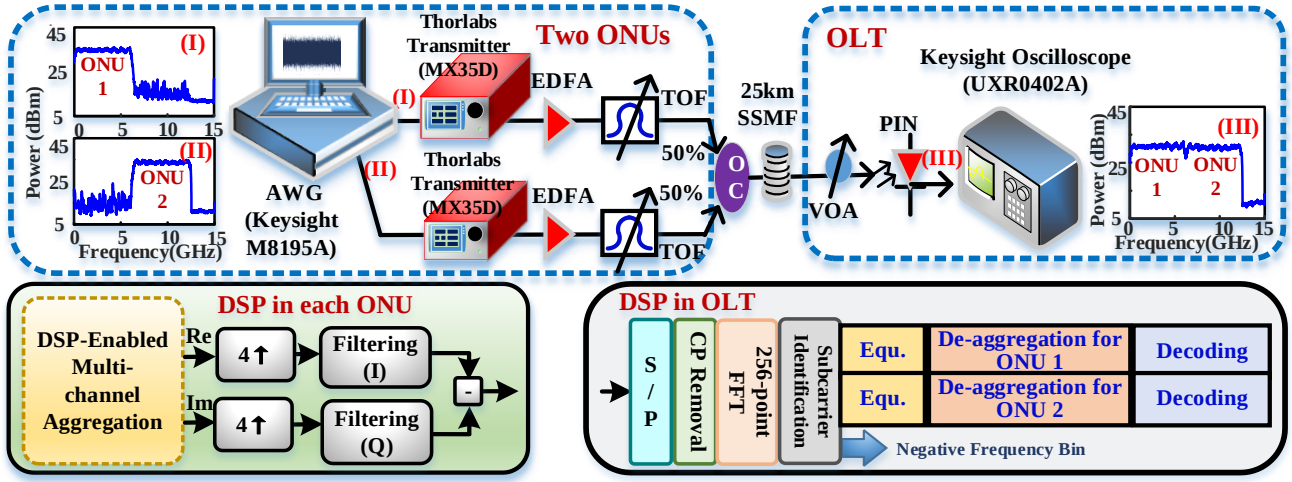

Fig. 3 Experimental setup of an upstream 25km PON incorporating the proposed P2MP flexible transceivers.

Furthermore, the proposed P2MP flexible transceivers fully support dynamic bandwidth/sub-wavelength allocations. Apart from above-discussed cases of dynamically activating/inactivating specific transmitters and/or specific sub-wavelengths of an individual transmitter, dynamic sub-wavelength alterations for an active DSP modulation function block of a specific transmitter are also achievable. This can be realized by dynamically altering, via SDN, the corresponding up-sampling factors and orthogonal digital filters in the corresponding transmitter DSP modulation function blocks and simultaneously modifying the corresponding large size FFT operation and subcarrier identification process in the receiver DSP. Through dynamic bandwidth/sub-wavelength allocations, the P2MP transmitters equipped with low-speed (high-speed) DACs can use low-frequency (high-frequency) sub-wavelengths for signal transmissions.

C. Transceiver DSP Complexity

For the proposed technique, if a large number of independent channels are conveyed by a specific sub-wavelength, the transceiver DSP complexity of the corresponding DSP function/sub-function block becomes large. Therefore, analyzing and evaluating the transceiver DSP complexity for a specific sub-wavelength accommodating various channel counts is important. In this paper, the DSP complexity is defined as the total number of required multiplication operations.

For the proposed P2MP flexible transmitters, the transmitter DSP complexity mainly arises from the IFFT operations involved in the DSP-enabled multi-channel aggregation operations and the orthogonal digital filtering operations. For the *i*-th sub-wavelength, to aggregate *R* independent channels, the DSP complexity of the required cascaded (*R*-1) IFFT operations can be calculated as,

$$O_{IFFT\_i\_Tx} = \sum_{v=1}^{R-1} (2^{v-1} N) \log_2 (2^v N) \qquad (7)$$

where ($2^v N$) is the size of the *v*-th IFFT operation as presented in Eq. (1). The DSP complexity of the two digital filtering operations can be expressed as,

$$O_{Filtering\_i\_Tx} = 2^R M_{k\_i} N(1+\varphi)\zeta_i \qquad (8)$$

where φ and ζ_i are the CP ratio and the digital filter length employed for the *i*-th sub-wavelength, respectively. As such, for the *i*-th sub-wavelength, the transmitter DSP complexity of the corresponding DSP modulation function block can be written as,

$$O_{i\_Tx} = O_{IFFT\_i\_Tx} + O_{Filtering\_i\_Tx} \qquad (9)$$

In the receiver DSPs, to de-aggregate *R* independent channels conveyed in the *i*-th sub-wavelength, the corresponding sub-function block performs cascaded (*R*-2) FFT operations, and the resulting receiver DSP complexity can be given by,

$$O_{FFT\_i\_Rx} = \sum_{v=1}^{R-2} (2^{v-1} N) \log_2 (2^v N) \qquad (10)$$

From the practical field programmable gate array (FPGA) implementation point of view, an IFFT/FFT operation can be implemented based on a butterfly scheme, where a 2^β-point IFFT/FFT operation is achievable by using two similar $2^{(\beta-1)}$-point IFFT/FFT operations. This implies that by enabling the outputs of the intermediate butterfly operations, a 2^β-point IFFT/FFT FPGA module may be used for flexibly realizing (2^Δ)-point IFFT/FFT operations with Δ=1, 2, …, β. As such, for the proposed technique, for each sub-wavelength, a single butterfly-based IFFT/FFT FPGA module with its size being dynamically configured to the required largest IFFT/FFT operation size would be sufficient for realizing the desired multi-channel aggregation and de-aggregation. Its required multiplier count is thus only related to the largest size of the required IFFT/FFT operations and is independent of the overall channel count, therefore leading to a logic resource-saving FPGA design.

TABLE I
CHANNEL BITRATE (GBPS)

ONU1	**CH1**	**CH2**	**CH3**	**CH4**
	3.4	3.4	6.6	14.8
ONU2	**CH1**	**CH2**	**CH3**	**CH4**
	3.4	3.4	6.2	14.1

III. P2MP FLEXIBLE TRANSCEIVER PERFORMANCES IN UPSTREAM IMDD PONS

To experimentally evaluate the performances of the proposed P2MP flexible transceivers, a representative upstream 55.3Gb/s @ 25km IMDD PON with two ONUs is utilized and the experimental setup is explicitly illustrated in Fig. 3. For simplicity, two sub-wavelengths are considered here, and each ONU transmits four independent channels over its corresponding sub-wavelength region.

In each ONU DSP, using the multi-channel aggregation technique illustrated in Fig. 2(a), three IFFT operations with their IFFT sizes of 16/32/64 are performed for aggregating four independent channels. A CP ratio of 1/16 is employed. The digital up-sampling factor is fixed at 4. A Hilbert-pair approach is utilized to produce two orthogonal digital filter pairs [20], and each ONU uses an orthogonal digital filter pair to locate its produced signal at the desired sub-wavelength. The digital filter length is taken to be 16 and the excess bandwidth factor is fixed at 0. After orthogonal digital filtering, a 1.2×digital oversampling operation, a digital-domain time delay operation and a signal clipping operation are performed for each ONU [19]. The digital domain time delay operation is performed to adjust the timing of two ONUs utilising the same clock. Such operation is a common practice widely adopted for achieving upstream ONU synchronisations in PONs incorporating DFM transceivers [19]. The clipping ratio is fixed at 12dB. A dual-channel 8-bit resolution arbitrary waveform generator (AWG, Keysight M8195A) operating at 30GSample/s is used to produce the two ONU upstream analogue signals. Each upstream analogue signal has a spectral bandwidth of 6.25GHz and an amplitude of 900mV. Their spectra are inserted in Fig. (I) and Fig. (II) of Fig. 3. Each of the produced upstream analogue signals consists of four independent channels. The modulation formats of each channel adaptively vary from BPSK to 64-QAM. The channel bitrates of the considered eight channels are listed in Table I. The ONU1 and ONU2 have aggregated ONU bitrates of 28.2Gb/s and 27.1Gb/s, respectively, thus giving rise to a total upstream bitrate of 55.3Gb/s over a 12.5GHz spectral region. To realize E/O conversions, two transmitters (Thorlabs MX35D) with a modulation bandwidth of 35GHz are utilized. Each transmitter contains a 15kHz linewidth free-running laser source and a 35GHz quadrature-biased Mach-Zehnder modulator (MZM). The two upstream wavelengths are fixed at 1564.6nm and 1565.4nm respectively, this gives rise to a 0.8nm upstream wavelength spacing to effectively mitigate the undesirable

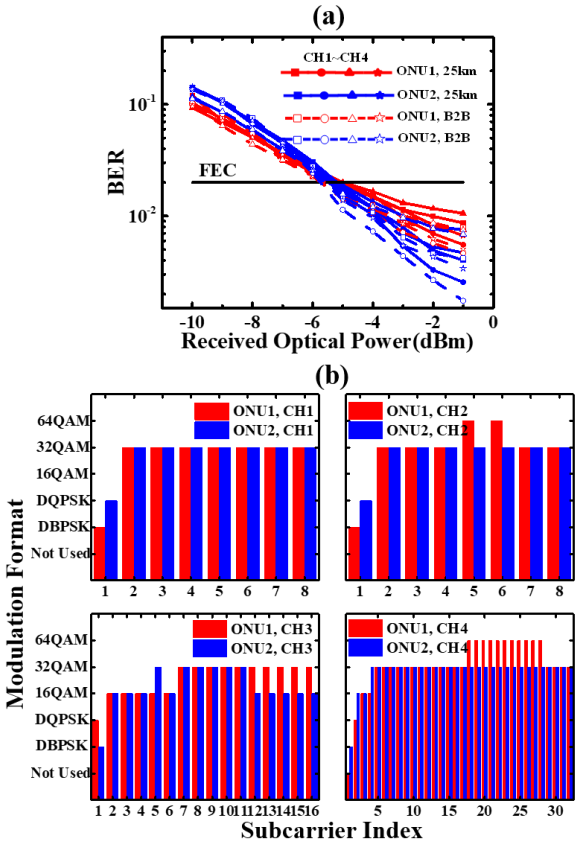

Fig. 4 (a) Measured BER transmission performances of BTB and 25km SSMF IMDD upstream PONs and (b) Optimised subcarrier bit allocation profile for each channel.

optical beating interference effect [19]. Two Erbium-doped fiber amplifiers (EDFAs) each followed by a 0.8nm bandwidth tuneable optical filter (TOF) sets the ONU output optical powers at 5dBm. For the PON considered in the paper, the EDFA and TOF are used in each ONU for achieving sufficiently high ONU optical launch powers to ensure that the dynamic changes of ONU optical launch powers can be fully explored. For achieving 50Gbit/s upstream transmissions in future 50G PONs, the utilisation of optical amplifiers may be allowable in the transceivers [23].

In the OLT, a 40GHz PIN detector (Thorlabs RXM40AF) converts the received two upstream optical signals to an electrical signal containing eight channels. After that, the received electrical signal is digitized by a 40GHz bandwidth digital sampling oscilloscope (Keysight UXR0402A) operating at 64GSample/s and then loaded to a computer for signal demodulation. As seen in Fig. 3, the OLT DSP procedures include S/P conversion, CP removal, 256-point FFT operation, conventional single-tap subcarrier equalization, multi-channel de-aggregation, and PSK/QAM decoding. In the multi-channel de-aggregation process, each ONU requires two FFT operations with the sizes of 32 and 16, respectively.

In the experiments, as shown in Fig. 3(III), a relatively flat upstream transmission system frequency response is achieved using the AWG and oscilloscope-embedded pre-compensation functions.

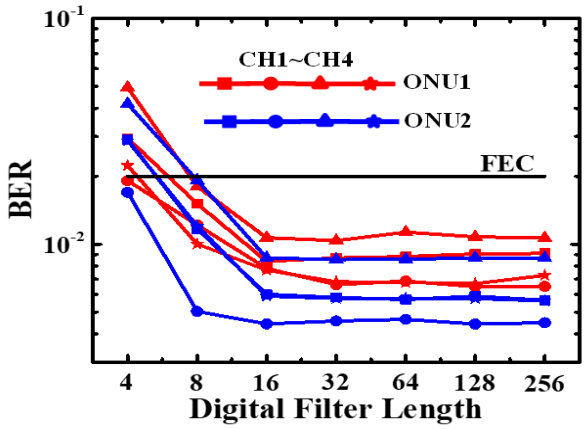

Fig. 5 Impacts of digital filter length variation on upstream PON transmission performances under received optical powers of -2dBm.

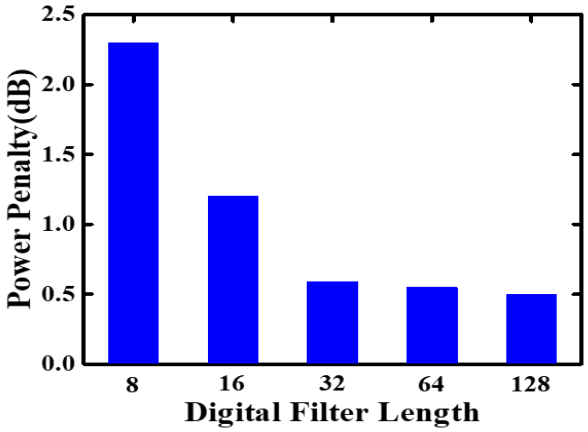

Fig. 6 Inter-SW channel interference effect-induced upstream power penalties.

A. *Upstream Transmission Performances*

Utilizing the above-stated experimental setups and signal generation/demodulation procedures, the upstream signal transmission performances of the considered eight channels are illustrated in Fig. 4. To explore the 25km standard single mode fiber (SSMF) transmission-induced upstream performance degradations at an adopted 20% overhead soft-decision forward error correction (SDFEC) threshold at a bit error rate (BER) of 2×10^{-2} (also used to define upstream power penalties in this paper), the back-to-back (B2B) upstream transmission performances of the considered eight channels are also presented in the same figure. It can be found that the upstream power penalties are <0.6dB for all the considered channels. The chromatic dispersion effect is negligible due to the pre-compensation techniques, CP insertion, and digital-domain time delay operation in the transmitters. ONU1 and ONU2 have similar BER performances due to adaptive bit-loading, and the optimised subcarrier bit allocation profile for each channel is presented in Fig. 4(b). In obtaining Fig. 4(b), for each involved channel, its optimum subcarrier bit allocation profile is achieved by adjusting all subcarrier modulation formats to ensure each subcarrier's BER at or close to the adopted FEC limit for a received optical power of -5dBm. Such upstream transmission performances and spectral efficiency (~4.4 bit/s/Hz) are similar to the results obtained using the DFM techniques [19, 24].

It is interesting to mention that the proposed technique is applicable for any modulation formats including conventional or differentially coded m-QAM/m-PSK. This is verified by the results presented in Fig. 4(b), where both differential BPSK/QPSK coding and conventional 8/16/64-QAM coding are considered for simplicity.

B. *Impacts of Orthogonal Digital Filter Characteristics*

The proposed P2MP flexible transceivers utilize orthogonal digital filtering to locate the aggregated signals at the desirable sub-wavelengths. As such, the orthogonal digital filter characteristics may have a direct impact on the performance of the proposed P2MP flexible transceivers. Considering the fact that a long digital filter length results in a large digital filter DSP
complexity, it is thus essential to identify the minimum digital filter length required to deliver an acceptable transmission performance. Based on the experimental parameter settings used in obtaining Fig. 4, the impacts of the digital filter length variation on the upstream transmission performances of the considered eight channels are illustrated in Fig. 5. In obtaining this figure, the received optical power is fixed at -2dBm and the fiber transmission distance is 25km. It can be seen that when the digital filter length is ≥16, further prolonging the digital filter length cannot considerably improve the upstream performances for all of the considered cases. This implies that the optimum digital filter length for the considered experimental parameter settings is 16, which is identical to the optimum digital filter length identified in the DFM technique-based upstream PONs offering the similar upstream transmission spectral efficiency [19, 24].

C. *Impacts of The Channel Interference Effect*

The use of the proposed P2MP flexible transceivers results in gapless FDM optical networks and each sub-wavelength is used for conveying multiple independent channels multiplexed in both the time and frequency domains, thus the channel interference effect may play an important role in determining the performances of the proposed P2MP flexible transceivers. For the upstream PON application scenario, for a specific channel, its suffered channel interferences mainly arise from the channels conveyed by its neighbour sub-wavelengths (here termed inter-SW channel interference) and the channels conveyed by the same sub-wavelength (here termed intra-SW channel interference).

Based on the experimental setup adopted in obtaining Fig. 5, for a digital filter length varying from 8 to 128, the inter-SW channel interference effect-induced upstream power penalties are explored in Fig. 6, which shows the upstream receiver sensitivity variations of four channels of one ONU between cases of the other ONU's four channels being switched on and off. In this paper, the upstream receiver sensitivity is defined as the minimum received optical power for a specific channel to achieve an upstream transmission BER at the FEC limit. As

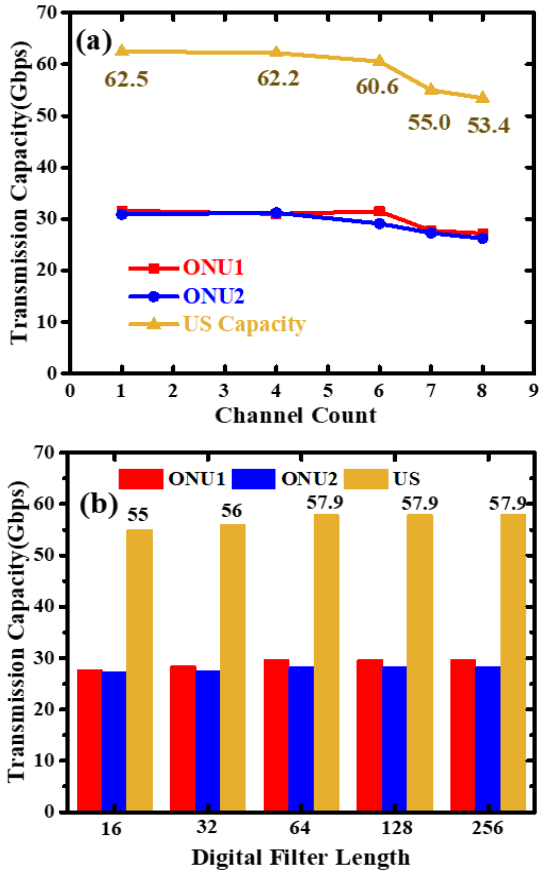

Fig. 7 (a) Impacts of intra-SW channel interference effect on upstream transmission capacity and (b) a relatively long digital filter length-induced upstream capacity improvements and each ONU accommodating 7 independent channels.

expected, the results show that prolonging the digital filter length can reduce the inter-SW channel interference effect. For the identified optimum digital filter length of 16, the inter-SW channel interference-induced upstream power penalties are <1.2dB. When the digital filter length is >16, further prolonging the digital filter length can only reduce the power penalty by <0.6dB. This indicates that, from the inter-SW channel interference reduction point of view, the optimum digital filter length is still 16 under the considered experimental parameter settings.

To explore the impacts of the intra-SW channel interference effect on upstream PON transmission performances, the maximum achievable upstream transmission capacity as a function of channel count are explored utilizing the experimental setup adopted in Section III(A). The measured results are presented in Fig. 7(a). The fiber transmission distance is 25km and the digital filter length is 16. It can be found that for each sub-wavelength, when the channel count is <6, the intra-SW channel interference effect-induced upstream transmission capacity degradations are almost negligible. When the channel count is >6, the intra-SW channel interference effect just slightly degrades the upstream transmission capacity. However, such upstream transmission capacity degradations can be mitigated by adopting a relatively long digital filter length. This is verified by Fig. 7(b), where each ONU transmits 7 independent channels. The figure shows that prolonging the digital filter length from 16 to 64 improves the upstream transmission capacity by ~5%. However, when the digital filter length is >64, the longer digital filter length-induced upstream transmission capacity improvements are negligible.

As shown in Fig. 6 and Fig. 7, the negligible inter-SW and intra-SW channel interference effects indicate that ONU-accommodated sub-wavelength count and the channel count conveyed by a specific sub-wavelength can be altered adaptively and dynamically without considerably compromising the upstream PON transmission capacity. As shown in the electrical signal spectrum of Fig. 3(III), no guard bands are inserted between these two signals occupying two adjacent sub-wavelengths. This is achievable because of the orthogonal digital filtering-induced considerable reductions in the intra-SW channel interferences.

IV. Differential ONU Optical Launch Power Dynamic Range

For practical hub-and-spoke optical access networks, such as PONs, the optical launch powers of different ONUs may be different. The differential ONU launch power may also play an important role in determining the upstream PON transmission performances. To explore the robustness of the proposed P2MP flexible transceiver-enabled PON upstream transmission performance against differential ONU launch power, the achievable differential ONU optical launch power dynamic ranges versus various aggregated upstream signal transmission capacities [19] are measured using the experimental setup adopted in Section III(A). The results are presented in Fig. 8. In this experimental setup, each ONU transmits four independent channels and adaptive bit-loading is utilized for each channel to adjust the aggregated upstream transmission capacity. The digital filter length is 16 and the fiber transmission distance is 25km. The received optical power is fixed at -2dBm.

It can be found in Fig. 8 that for the considered PONs incorporating the proposed P2MP flexible transceivers, the maximum achievable aggregated upstream signal transmission capacity is ~62.2Gb/s, which leads to an upstream transmission spectral efficiency of ~4.97bit/s/Hz. Increasing the ONU launch power dynamic range by 1dB gives rise to ~1.97Gb/s reductions in aggregated upstream transmission capacity or ~0.16bit/s/Hz reductions in upstream transmission spectral efficiency. It also reveals that the proposed P2MP flexible transceivers can offer arbitrary differential ONU launch power dynamic ranges by slightly compromising the aggregated upstream signal transmission capacity.

It is also interesting to find that the proposed P2MP flexible transceivers and the conventional DFM transceivers are subject to similar upstream transmission spectral efficiency reductions for achieving an 1dB increase in the ONU launch power dynamic range [19, 24].

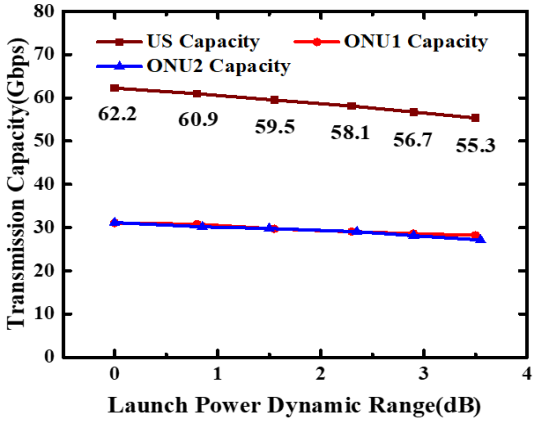

Fig. 8 Transmission capacity versus differential ONU optical launch power dynamic range for a received optical power of -2dBm.

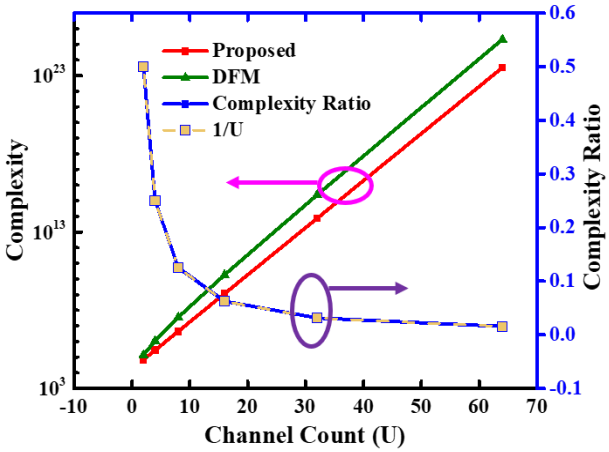

Fig. 9 ONU transmitter DSP complexity comparisons between proposed techniques and conventional DFM techniques.

V. Transmitter DSP Complexity

In an upstream PON incorporating the proposed P2MP flexible transceivers, for each individual sub-wavelength, the cascaded IFFT (FFT) operations are performed for realizing the desired multi-channel aggregations (de-aggregations). Because the IFFT and FFT operations have similar DSP complexities and the orthogonal digital filtering operations are performed in the ONU transmitter DSPs only, in this section, special attention is thus given to analyzing the ONU transmitter DSP complexity only.

In an upstream PON, according to the transceiver DSP complexity analysis presented in Section II(C), the transmitter DSP complexity of a single ONU for accommodating various channel counts is evaluated and presented in Fig. 9. The results are calculated by taking into account the following assumptions: 1) the PON system accommodates 64 ONUs each allocated a single sub-wavelength of the same bandwidth for signal transmission, 2) for the multi-channel aggregation in the transmitter DSP, the size of the first IFFT operation is 16, 3) the CP ratio is fixed at 1/16, and 4) the digital filter length is taken to be 16.

To explicitly demonstrate the advantages of the proposed technique in reducing the transmitter DSP complexity, the DSP complexity of a single DFM transmitter accommodating similar channel counts and channel bitrates is also calculated and plotted in Fig. 9 for comparison. For the DFM transmitters, the DSP complexity mainly arises from the parallel orthogonal digital filtering operations for multi-channel aggregations [20].

The DSP complexity ratios between the proposed P2MP flexible transmitters and the conventional DFM transmitters are illustrated in Fig. 9. It can be found that when the channel count is *U*, the proposed techniques can reduce the ONU transmitter DSP complexity by a factor of *U*. This reveals that the proposed technique outperforms the DFM technique in terms of reducing the transmitter DSP complexity, and such superiority becomes more pronounced when a large number of independent channels are accommodated.

The subcarrier multiplexing techniques [25] utilize digital filtering to realize Nyquist-shaping and each complex signal requires two digital filtering operations. As such, for a given digital filter length, the subcarrier multiplexing technique and the orthogonal digital filtering-based multi-channel aggregation technique should have similar digital filter DSP complexity. As shown in Fig. 9, the cascaded IFFT/FFT-enabled multi-channel aggregation/de-aggregation techniques involved in the proposed transceivers outperform the orthogonal digital filtering-based multi-channel aggregation/de-aggregation technique in terms of DSP complexity. Thus, the cascaded IFFT/FFT-enabled multi-channel aggregation/de-aggregation techniques may lower the DSP complexity in comparison with the subcarrier multiplexing technique.

VI. Network Security Evaluations

For the proposed P2MP flexible transceivers, in each sub-wavelength, the conveyed multiple independent channels are multiplexed in both the time domain and the frequency domain at various DSP stages, this hinders eavesdroppers from illegally separating a channel in each individual sub-wavelength without the knowledge of transceiver DSP configurations.

The upstream PON experimental setup adopted in obtaining Fig. 4 is used to evaluate the security of the proposed technique. The temporal waveforms and corresponding signal spectra of the directly detected upstream signals are shown in Fig. 10(a) and Fig. 10(b). It can be found that the noise-like features of the illegally captured upstream signal temporal waveforms prevent eavesdroppers from obtaining the key transceiver DSP configuration parameters for demodulating the illegally captured signals, the parameters include, for example, channel count of each individual sub-wavelength, data-bearing subcarrier count in each channel and subcarrier modulation formats in each channel.

More importantly, after the large-size FFT operation and subcarrier equalization process, for each individual sub-wavelength, the constellations and the temporal waveforms of all the subcarriers are chaotic. This is verified by Figs. 10 (c)~(f), where for the considered experimental setup, the 15-th subcarrier of each ONU upstream signal is presented. Such chaotic subcarrier temporal waveforms and constellations further prevent eavesdroppers from illegally obtaining

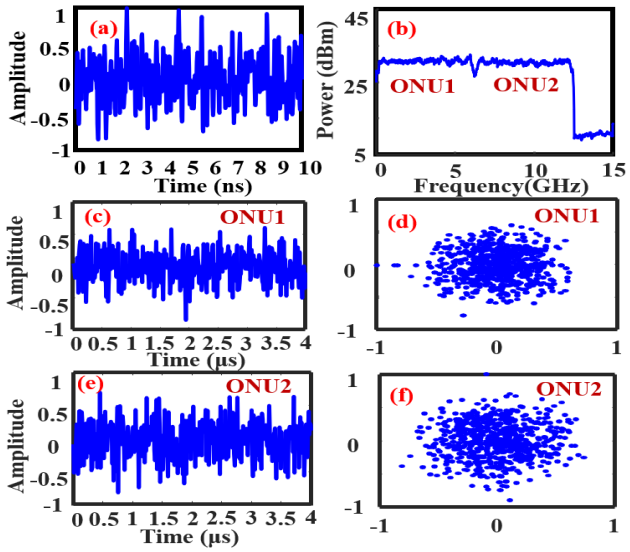

Fig. 10 (a) and (b) Temporal waveform and signal spectrum of an illegally detected upstream signal; (c)/(d) and (e)/(f) Temporal waveforms and constellations of 15-th subcarriers of two ONUs prior to channel de-aggregation.

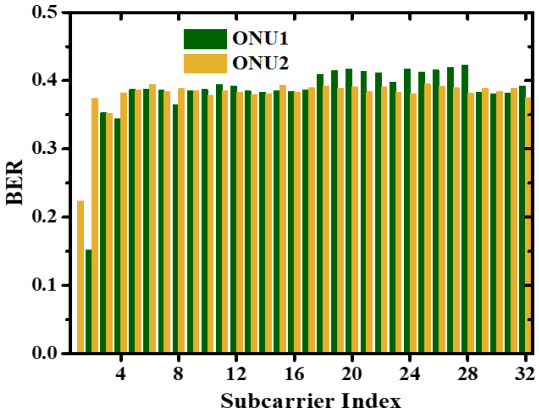

Fig. 11 Subcarrier BER performances of illegally obtained CH4 signals.

transceiver DSP configuration parameters for both channel de-aggregation and signal demodulation.

Based on the considered upstream PON experimental setups, using the subcarriers illegally obtained after performing the large-size FFT operation and subcarrier equalization process to obtain the 4-th channel (CH4) data/information of each ONU, the subcarrier BER performances of the illegally obtained CH4 signals are measured and presented in Fig. 11. It implies that without successfully performing the channel de-aggregation utilising the transceiver DSP configuration, it is almost impossible for eavesdroppers to illegally obtain the transmitted user data.

The above results indicate that the proposed P2MP flexible transceivers offer additional physical layer network security. It is also worth highlighting that the proposed techniques are fully compatible with all existing high layer network encryption techniques such as IPsec [26] at layer 3 and MACsec [27] at layer 2 of the Open Systems Interconnection model. From a practical application point of view, the proposed P2MP flexible transceivers can be deployed together with these high layer network encryption techniques to comprehensively protect the networks from the high layer all the way down the physical layer.

For the proposed technique, dynamic bandwidth allocation is achieved by dynamically configuring transceiver's DSP. To securely transmit the transceiver DSP configuration information over networks, the transceiver DSP configuration information can be encrypted using existing network security techniques, such as IPsec and MACsec.

The proposed P2MP flexible transceivers are suitable for any types of transceiver-embedded lasers, intensity modulators and photon detectors as well as network topologies. To effectively highlight the key features associated with the proposed transceivers, all unwanted effects must be suppressed as much as possible, which for IMDD PONs, include, for example, the effects associated with laser linewidth and intensity modulation-induced frequency chirp, practical hardware impairments and their interplay, as well as direct-detection-induced signal-to-signal beating interference (SSBI) [28]. Except for the SSBI effect, the use of high-quality and expensive components is effective in suppressing all of the abovementioned unwanted effects. As a direct result, the performances of the IMDD PONs based on such components are mainly limited by the SSBI effect. Given the fact that the recently published DSP-based IMDD transmission system linearization techniques [28] can effectively reduce the SSBI effect, significant IMDD PON performance improvements in both signal transmission capacity and power budget are thus envisaged when use is made of the linearization technique in the proposed transceivers. Of course, low-cost electrical and optical components are preferred for practical implementation of the technique. The achievable performances of the proposed transceivers incorporating low-cost electrical and optical components of various characteristics are currently being explored in our research lab, and the corresponding results will be published elsewhere in due course.

When the proposed technique is sufficiently mature for practical implementation, its implementation in 50G PONs [23] just needs to upgrade and re-configurate its transceiver DSPs without requiring extra optical and electoral components. As such, the technique is potentially cost-effective. It should also be noted that, for practical implementations of the proposed technique in 50G PON application scenarios [23], further explorations and evaluations of the technique are required. However, to improve the technique's power budget, ONU launch power dynamic range and transmission distance for 50G PON applications, in addition to the IMDD transmission system linearization techniques, some conventional approaches may be considered, including, for example, 1) increasing the ONU launch power [29], 2) employing a low-noise avalanche photo-diode (APD) in the receiver [29], 3) using a pre-amplifier prior to optical-electrical conversion in the receiver [29].

VII. Conclusions

A novel P2MP flexible transceiver has been proposed, experimentally demonstrated and optimised in an upstream

55.3Gb/s over 25km IMDD PON. The transceiver incorporates a new cascaded IFFT/FFT-based multi-channel aggregation/de-aggregation technique and an orthogonal digital filtering technique to allow each individual ONU to dynamically transmit an arbitrary number of independent channels over each of its allocated sub-wavelengths.

In comparison with the conventional DFM techniques, the proposed techniques have two major advantages, 1) significantly reducing the transmitter DSP complexity by a factor that is approximate to aggregated channel count, and 2) offering additional physical layer security by preventing eavesdroppers from de-aggregating and demodulating the illegally captured channels without the knowledge of the transceiver DSP configurations. These advantages are achieved without requiring a relatively long digital filter length and considerably compromising upstream transmission performances/spectral efficiency and differential ONU optical launch power dynamic ranges.

In the considered 25km upstream PONs, the upstream signal transmission-induced power penalties are <0.6dB, and the optimum digital filter length is identified to be 16. By utilizing the identified optimum digital filter length, the inter-SW channel interference-induced upstream power penalties are <1.2dB, and the intra-SW channel interference-induced upstream capacity degradations are negligible if the channel count is <6. When the channel count is >6, the maximum achievable upstream capacity is slightly decreased, which, however, can be mitigated by using a relatively large digital filter length. An arbitrary differential ONU optical launch power dynamic range is achievable by slightly compromising the upstream transmission spectral efficiency. For the considered 25km PONs with a maximum achievable upstream spectral efficiency of ~4.97bit/s/Hz, every 1dB increase in the ONU optical launch power dynamic range can result in ~0.16bit/s/Hz reductions in upstream transmission spectral efficiency.

REFERENCES

[1] H. Okazaki, Y. Suzuki, S. Suyama, and Takahiro Asai, "THz transport technologies and strategists beyond 5G/6G Systems," *Proc. Opt. Fiber Commun.*, San Diego, CA, USA, 2022, Paper M3C.6.

[2] X. Cheng, Z. Huang, and L. Bai, "Channel nonstationarity and consistency for beyond 5G and 6G: a survey," *IEEE Commun. Surveys Tuts.*, vol. 24, no. 3, pp. 1634-1669, 2022.

[3] Y. J. Huang, G. T. Lin, P. H. Ting, C. C. Wei, S. Chi, and C. T. Lin, "Analog mobile fronthaul supporting 128 RF chain with nonlinear compensator for B5G and 6G Ma-MIMO beamforming," *J. Light. Technol*., vol. 40, no. 20, pp. 6867-6874, Oct. 2022.

[4] D. Dass, A. Delmade, L. Barry, C. G. H. Roeloffzen, D. Geuzebroek, and C. Browning, "Wavelength & mm-Wave flexible converged optical fronthaul with a low noise Si-based integrated dual laser source," *J. Light. Technol*., vol. 40, no. 10, pp. 3307-3315, May 2022.

[5] M. Wang, G. Simon, L. A. Neto, I. Amigo, L. Nuaymi, and P. Chanclou, "SDN East–West cooperation in a converged fixed-mobile optical access network: enabling 5G slicing capabilities," *J. Opt. Commun. Netw.*, vol. 14, no. 7, pp. 540-549, Jul. 2022.

[6] R. Borkowski, M. Straub, Y. Ou, Y. Lefevre, Ž. L. Jeli´c, W. Lanneer, N. Kaneda, A. Mahadevan, V. Hückstädt, D. V. Veen, V. Houtsma, W. Coomans, R. Bonk, and J. Maes, "FLCS-PON - a 100 Gbit/s flexible passive optical network: concepts and field trial," *J. Light. Technol*., vol. 39, no. 16, pp. 5314-5324, Aug. 2021.

[7] M. M. Hosseini1, J. Pedro, N. Costa, A. Napoli, J. E. Prilepsky, and S. K. Turitsyn, "Optimized physical design of metro aggregation networks using point to multipoint transceivers," *Proc. Opt. Fiber Commun.,* San Diego, CA, USA, 2022, Paper W3F.2.

[8] D. Welch, A. Napoli, J. B¨ack, S. Buggaveeti, C. Castro, A. Chase, X. Chen, V. Dominic, T. Duthel, T. A. Eriksson, Sezer Erkilinç, P. Evans, C. R. S. Fludger, B. Foo, T. Frost, P. Gavrilovic, S. J. Hand, A. Kakkar, A. Kumpera, V. Lal, R. Maher, F. Marques, F. Masoud, A. Mathur, R. Milano, M. I. Olmedo, M. Olson, D. Pavinski, J. Pedro, A. Rashidinejad, P. Samra, W. Sande, A. Somani, H. Sun, N. Swenson, H. S. Tsai, A. Yekani, J. Zhang, and M. Ziari, "Digital subcarrier multiplexing: enabling software-configurable optical networks," *J. Light. Technol*., early access, 2022.

[9] A. Napoli, Z. Stevkovski, J. D. M. Jiménez, E. J. E. Zuleta, J. Bäck, J. Pedro, J. Rodriguez, R. Diaz, J. Carrallo, A. Mathur, J. P. F.-P. Gimenez, F. Masoud, and D. Welch, "Enabling router bypass and saving cost using point-to-multipoint transceivers for traffic aggregation," *Proc. Opt. Fiber Commun.,* San Diego, CA, USA, 2022, Paper W3F.5.

[10] Z. Zhou, J. Wei, K. A. Clark, E. Sillekens, C. Deakin, R. Sohanpal, Y. Luo, R. Slavík, and Z. Liu, "Multipoint-to-point data aggregation using a single receiver and frequency-multiplexed intensity-modulated ONUs," *Proc. Opt. Fiber Commun.,* San Diego, CA, USA, 2022, Paper Tu2G.4.

[11] Infinera, solution brief, XR Optics, innovative point-to-multipoint coherent that slashes aggregation network TCO, 2022. https://www.infinera.com/innovation/xr-optics.

[12] D. Welch, A. Napoli, J. Bäck, W. Sande, J. Pedro, F. Masoud, C. Fludger, T. Duthel, H. Sun, S. J. Hand, T.-K. Chiang, A. Chase, A. Mathur, T. A. Eriksson, M. Plantare, M. Olson, S. Voll, and K.-T. Wu, "Point-to-multipoint optical networks using coherent digital subcarriers," *J. Light. Technol*., vol. 39, no. 16, pp. 5232-5247, Aug. 2021.

[13] M. M. Hosseini, J. Pedro, A. Napoli, N. Costa, J. E. Prilepsky, and S. K. Turitsyn, "Optimization of survivable filterless optical networks exploiting digital subcarrier multiplexing," *J. Opt. Commun. Netw.*, vol. 14, no. 7, pp. 586-594, Jul. 2022.

[14] P. Pavon-Marino, N. Skorin-Kapov, M. V. Bueno-Delgado, J. Back, and A. Napoli, "On the benefits of point-to-multipoint coherent optics for multilayer capacity planning in ring networks with varying traffic profiles," *J. Opt. Commun. Netw.*, vol. 14, no. 5, pp. B30-B44, May 2022.

[15] E. Al-Rawachy, R. P. Giddings, and J. M. Tang, "Experimental demonstration of a real-time digital filter multiple access PON with low complexity DSP-based interference cancellation," *J. Light. Technol.*, vol. 37, no. 17, pp. 4315–4329, Sep. 2019.

[16] M. L. Deng, T. Mamadou, Z. B. Xing, X. Kang, Z. R. Luo, J. W. Shi, and L. Wang, "Digital orthogonal filtering-enabled synchronous transmissions of I/Q waveforms and control words for bandwidth-efficient and low-complexity mobile fronthaul," *Proc. Opt. Fiber Commun.*, Francisco, CA, USA, 2021, Paper F1D.2.

[17] W. Jin, A. Sankoh, Y. X. Dong, Z. Q. Zhong, R. P. Giddings, M. O'Sullivan, J. Lee, T. Durrant, and J. M. Tang, "Hybrid SSB OFDM-digital filter multiple access PONs," *J. Light. Technol.*, vol. 38, no. 8, pp. 2095–2105, Jan. 2020.

[18] A. Sankoh, W. Jin, Z. Zhong, J. He, Y. Hong, R. P. Giddings, I. Pierce, M. O'Sullivan, J. Lee, T. Durrant, J. Tang, "Hybrid OFDM-digital filter multiple access PONs utilizing spectrally overlapped digital orthogonal filtering," *IEEE Photon. J.*, vol. 12, no. 5, pp. 7905311, Otc. 2020.

[19] Z. Q. Zhong, W. Jin, S. Jiang, J. X. He, D. Chang, Y. H. Hong, R. P. Giddings, X. Q. Jin, M. O'Sullivan, T. Durrant, J. Trewern, G. Mariani, and J. M. Tang, "Concurrent inter-ONU communications for next generation mobile fronthauls based on IMDD hybrid SSB OFDM-DFMA PONs," *J. Light. Technol.*, vol. 39, no. 23, pp. 7360-7369, Dec. 2021.

[20] W. Jin, Z. Q. Zhong, S. Jiang, J. X. He, S. H. Hu, D. Chang, R. P. Giddings, Y. H. Hong, X. Q. Jin, M. O'Sullivan, T. Durrant, J. Trewern, G. Mariani, and J. M. Tang, "Experimental demonstrations of DSP-enabled flexibility, adaptability and elasticity of multi-channel >72Gb/s over 25 km IMDD transmission systems," *Opt. Express*, vol. 29, no. 25, pp. 41363-41377, Dec. 2021.

[21] M. Xu, J.-H. Yan, J. Zhang, F. Lu, J. Wang, L. Cheng, D. Guidotti, and G.-K. Chang, "Bidirectional fiber-wireless access technology for 5G mobile spectral aggregation and cell densification," *J. Opt. Commun. Netw*., vol. 8, no. 12, pp. B104–B110, Dec. 2016.

[22] W. Jin, Z. Q. Zhong, S. Jiang, J. X. He, D. Chang, Y. H. Hong, R. P. Giddings, X. Q. Jin, M. O'Sullivan, T. Durrant, J. Trewern, G. Mariani, and J. M. Tang, "Rectangular orthogonal digital filter banks based on extended Gaussian functions," *J. Light. Technol.*, vol. 40, no. 12, pp. 3709-

3722, Jun. 2022.
[23] Dezhi Zhang, Dekun Liu, Xuming Wu, and Derek Nesset, “Progress of ITU-T higher speed passive optical network (50G-PON) standardization,” *J. Opt. Commun. Netw.*, vol. 12, no. 10, pp. D99–D108, Oct. 2020.
[24] Z. Zhong, W. Jin, S. Jiang, J. He, D. Chang, R. Giddings, Y. Hong, M. O’Sullivan, T. Durrant, G. Mariani, J. Trewern, and J. Tang, “Experimental demonstrations of concurrent adaptive inter-ONU and upstream communications in IMDD hybrid SSB OFDM-DFMA PONs,” *Proc. Opt. Fiber Commun.*, Francisco, CA, USA, 2021, Paper F4I.5.
[25] Haide Wang, Ji Zhou, Jinlong Wei, Dong Guo, Yuanhua Feng, Weiping Liu, Changyuan Yu, Dawei Wang, and Zhaohui Li, “Multi-Rate Nyquist-SCM for C-Band 100 Gbit/s Signal Over 50 km Dispersion-Uncompensated Link,” *J. Light. Technol.*, vol. 40, no. 7, pp. 1930–1936, Apr. 2022.
[26] IEEE Std 2030.102.1-2020, “IEEE Standard for Interoperability of Internet Protocol Security (IPsec) Utilized within Utility Control Systems”, Dec. 3, 2020.
[27] IEEE Std 802.1AE-2018 (Revision of IEEE Std 802.1AE-2006), “IEEE Standard for Local and metropolitan area networks-Media Access Control (MAC) Security”, Sep. 27, 2018.
[28] S. Hu, J. Zhang, J. Tang, W. Jin, R. Giddings, and K. Qiu, “Data-aided iterative algorithms for linearizing IM/DD optical transmission systems,” *J. Light. Technol.*, vol. 39, no. 9, pp. 2864–2872, May 2021.
[29] René Bonk, Dan Geng, Denis Khotimsky, Dekun Liu, Xiang Liu, Yuanqiu Luo, Derek Nesset, Vladimir Oksman, Rainer Strobel, Werner Van Hoof, and Jun Shan Wey, “50G-PON: The First ITU-T Higher-Speed PON System,” *IEEE Communications Magazine*, vol. 60, no. 3, pp. 48–54, Mar. 2022.